EPJ Web of Conferences **61**, 02005 (2013)
DOI: 10.1051/epjconf/20136102005

Rayleigh-Taylor and Richtmyer-Meshkov Instabilities in Relativistic Hydrodynamic Jets

Jin Matsumoto[1,2,a] and Youhei Masada[3,b]

[1] *Center for Computational Astrophysics, National Astronomical Observatory of Japan, Tokyo, Japan*
[2] *Astrophysical Big Bang Laboratory, RIKEN, Wako, Japan*
[3] *Graduate School of System Informatics, Department of Computational Science, Kobe University, Kobe, Japan*

Abstract. We investigate the stability of relativistic jets using three-dimensional hydrodynamic simulations. The propagation of relativistic flow that is continuously injected from the boundary of computational domain into a uniform ambient medium is solved. An intriguing finding in our study is that Rayleigh-Taylor and Richtmyer-Meshkov type instabilities grow at the interface between the jet and surrounding medium as a result of spontaneously induced radial oscillating motion. It is powered by in situ energy conversion between the thermal and bulk kinetic energies of the jet. From complementary two-dimensional simulations of transverse structure of the jet, we find the effective inertia ratio of the jet to the surrounding medium determines a threshold for the onset of instabilities. The mixing between light faster jet and slow heavier external matters due to these instabilities causes the deceleration of the jet.

1 Introduction

Morphology is one of the most fundamental property of the relativistic jet. The formation of the hydrodynamic/magnetohydrodynamic structure due to the interaction between the jet and external medium is responsible for the morphology of the jet. Observational, theoretical, and numerical works have extensively been performed in order to understand the jet morphology in various high-energy astrophysical phenomena, such as active galactic nuclei (AGNs) [1, 2], microquasars [3], and gannma-ray bursts (GRBs) [4, 5].

Basic features of the propagation and morphology of the jet are well established by analytical and numerical studies [6–10] although the formation mechanism of relativistic jets is a long-standing problem in AGNs, microquasars, and GRB jets (but see, e.g., [11–14]). Figure 1(a) schematically depicts the traditional picture of the relativistic jet propagating through the ambient medium. The propagation of the jet generates a bow shock structure at the head of the jet. The jet boring through the ambient medium is not in direct contact with the undisturbed ambient medium, but rather is enveloped in a hot cocoon consisting of shocked jet material and shocked ambient medium. Inside the jet, reconfinement shocks are formed due to a pressure mismatch between the jet and cocoon [15, 16].

Instabilities in fluid dynamics including magnetic field play an important role in and drastically change the morphology and stability of the relativistic jet through the interaction between the jet and external medium. The disruption and deceleration of the relativistic jet may be attributed to the Kelvin-Helmholtz instability driven by velocity shear at the interface between the jet and the surrounding medium [17–19]. Strongly magnetized jet, in which toroidal magnetic field is dominant is subjected to the kink mode of current-driven instability [20]. The rotation-induced Rayleigh–Taylor-type instability in a rotating two-component jet may also impact on the deceleration and decollimation of the jet [21, 22].

Even without the rotation, the relativistic jet potentially becomes unstable to the Rayleigh-Taylor instability [23]. A radial inertia force, which naturally arises from a pressure mismatch between the jet and cocoon when the jet propagates through the ambient medium, drives the radial oscillating motion of the jet, yielding the reconfinement region inside the jet [7, 24]. This radial inertia force triggers the Rayleigh-Taylor instability at the jet interface.

When considering the non-axisymmetric evolution of the jet, the radial oscillation-induced Rayleigh-Taylor instability at the interface of the jet might have a potential impact on the deformation and morphology of the relativistic jet. In these proceedings, the nonlinear development of the relativistic jet is studied using three-dimensional (3D) special relativistic hydrodynamic (SRHD) simulations.

2 Numerical Method

2.1 Basic Equations

We numerically solve the nonlinear development of a relativistic jet in a cylindrical coordinate system (r, θ, z). As-

[a] e-mail: jin@cfca.jp,jin.matsumoto@riken.jp
[b] e-mail: ymasada@harbor.kobe-u.ac.jp

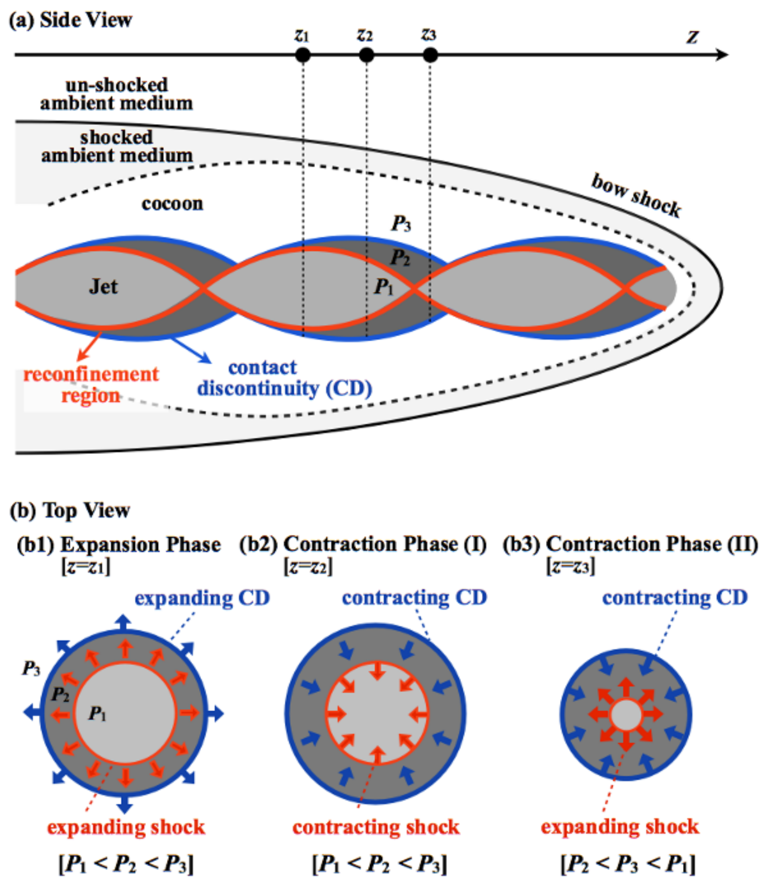

Figure 1. Schematic picture of the jet propagating through the ambient medium (see Figure 1 in Ref. [23]). Top and bottom panels are side and top views of the jet, respectively.

suming an ideal gas law with a ratio of specific heats $\Gamma = 4/3$, the governing equations we solved are

$$\frac{\partial}{\partial t}(\gamma\rho) + \nabla \cdot (\gamma\rho\mathbf{v}) = 0\,, \quad (1)$$

$$\frac{\partial}{\partial t}(\gamma^2\rho h\mathbf{v}) + \nabla \cdot (\gamma^2\rho h\mathbf{v}\mathbf{v} + Pc^2\mathbf{I}) = 0\,, \quad (2)$$

$$\frac{\partial}{\partial t}(\gamma^2\rho h - P) + \nabla \cdot (\gamma^2\rho h\mathbf{v}) = 0\,, \quad (3)$$

where $\gamma = 1/\sqrt{1-(v_r/c)^2-(v_\theta/c)^2-(v_z/c)^2}$ is the Lorentz factor and $h = 1 + \Gamma P/(\Gamma-1)\rho c^2$ is the specific enthalpy. The other symbols have their usual meanings.

A relativistic HLLC scheme is used to solve the SRHD equations (1)–(3) [25]. The primitive variables are calculated from the conservative variables following the method of Ref. [26]. We use a MUSCL-type interpolation method to attain second-order accuracy in space while the temporal accuracy obtains second-order by using Runge-Kutta time integration.

2.2 Numeric Model and Setup

Relativistically hot flow is continuously injected into the ambient medium from the lower boundary of the computational domain. We assume the relativistically hot jet with greater pressure and lower rest-mass energy density than the ambient medium. The rest-mass energy density and pressure of the injected jet are chosen as $\rho_{\mathrm{jet},0}c^2 = 0.1$ and $P_{\mathrm{jet},0} = 1$, respectively. Those of the ambient medium are $\rho_{\mathrm{amb},0}c^2 = 1$ and $P_{\mathrm{amb},0} = 0.1$. In addition, the jet velocity of the injected flow from the lower boundary to the z-direction is relativistic $v_z = 0.99c$, with a Lorentz factor of $\gamma_{\mathrm{jet},0} \sim 7$. The ambient medium does not move.

The normalization units in length, velocity, time, and energy density are chosen as the jet radius of the injected flow at the lower boundary $r_{\mathrm{jet},0}$, light speed c, light crossing time over the jet radius $r_{\mathrm{jet},0}/c$, and rest mass energy density in the ambient medium $\rho_{\mathrm{amb},0}c^2$. We use a uniformly spaced grid in cylindrical coordinates consisting of $450 \times 160 \times 1000$ zones in r-, θ-, and z-directions. The computational domain spans $0 \le r/r_{\mathrm{jet},0} \le 30$, $0 \le \theta \le 2\pi$, and $0 \le z/r_{\mathrm{jet},0} \le 1000$. The jet radius of the injected flow at the lower boundary is resolved by 15 numeric cells. The 30 uniform logarithmic grids are spaced in the range of $30 < r/r_{\mathrm{jet},0} < 100$. At the lower boundary hydrodynamic variables are fixed inside the jet injection region ($0 < r/r_{\mathrm{jet},0} < 1$), while the boundary conditions are reflective outside the jet injection region. An outflow (zero gradient) boundary condition is imposed on the outer boundary of the domain. By introducing small-amplitude (1%) random pressure perturbations to the injected relativistic flow and the ambient medium, the simulation is initiated.

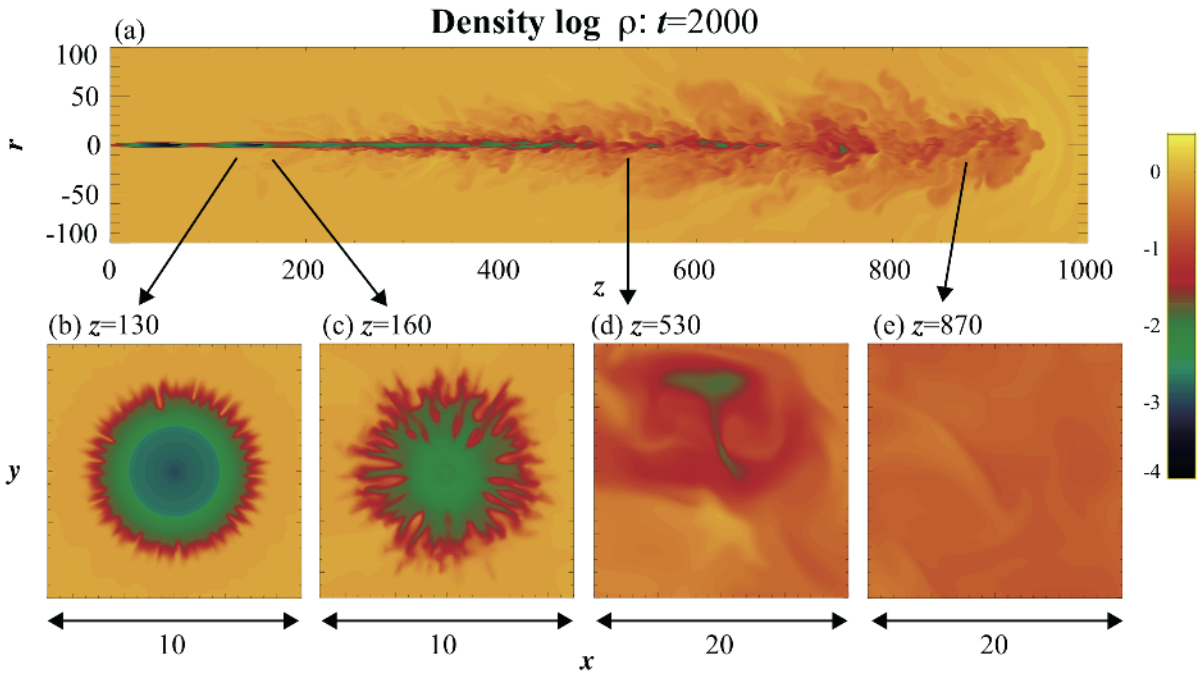

Figure 2. Snapshots of the 2D spatial distribution of the density in the 3D calculation for the propagation of the relativistic jet through the uniform ambient medium when $t = 2000$. Panel (a) shows the 2D cut in the $r - z$ plane of the density distribution. Panel (b)-(e) represent 2D cuts in the $r - \theta$ $(x - y)$ plane where $z = 130$, 160, 530, and 870.

3 Results

3.1 3D Jet Propagation

Figure 2 shows snapshots of the two-dimensional (2D) spatial distribution of the density in the 3D calculation for the propagation of the relativistically hot jet through the uniform ambient medium when $t = 2000$. Panel (a) shows the 2D cut of rest-mass density along the propagation axis. Panel (b)-(e) represent 2D transversal cuts of the rest-mass density where $z = 130$, 160, 530, and 870, respectively.

The jet propagates through the ambient medium by pushing the ambient matter in front of the jet, leading to the formation of a forward shock. A contact discontinuity separates the jet and surrounding medium. One can find that the jet-surrounding medium interface becomes unstable and Rayleigh-Taylor type fingers appear in Figure 2(b). The amplitude of the corrugated jet-surrounding medium interface grows at $z = 160$. The inward pressure-gradient force acting on the jet-surrounding medium interface induces the Rayleigh-Taylor instability.

The material mixing due to the deformation of the interface between the jet and surrounding medium (see Figure 1(d) and 1(e)) leads to the jet disruption and the deceleration of the jet. The flow velocity of the jet in the region where $z/r_{\rm jet,0} \sim 900$ is roughly $0.7c$ although that of the injected relativistic flow at the lower boundary is $0.99c$. The Bernoulli's constant γh, which is conserved when the fluid of the relativistic jet changes adiabatically, behind the jet head also decreases to 10 due to the mixing between light faster jet and slow heavier external matters. This is only 4 % of that of the injected relativistically hot flow at the lower boundary.

3.2 Stability of Relativistic Jets

In this section, we investigate the deformation process of the interface between the jet and surrounding medium when a radial inertia force acts on the interface through the 3D SRHD simulation. We focus on the temporal evolution of the interface between a cylindrical jet and the surrounding medium within a periodic computational box to the jet direction.

For our initial conditions, we initially set the cylindrical jet surround by a gas in 3D calculation domain (see Figure 3(a)). The initial rest mass energy density and pressure in the jet are chosen as $\rho_{\rm jet,0}c^2 = 0.1$ and $P_{\rm jet,0} = 1$, respectively. Those of the external medium are $\rho_{\rm ext,0}c^2 = 1$ and $P_{\rm ext,0} = 0.1$. The jet velocity to the z-direction is relativistic $v_{\rm jet,0} = 0.99c$ (the corresponding Lorentz factor is $\gamma_{\rm jet,0} \sim 7$). The external medium does not move and the transverse components (v_r and v_θ) of the velocity are set to be zero initially in the calculation domain. We have considered a model with a 1% perturbation in the pressure in the computational box.

Since the jet is initially overpressured in our model, it starts to expand adiabatically in the radial direction. The repeated in situ energy conversion between the thermal and bulk kinetic energies of the jet induces naturally the radial inertia force inside the jet and the radial oscillating motion of the jet [24].

We use a uniformly spaced grid in cylindrical coordinates consisting of $320 \times 200 \times 320$ zones in r-, θ-, and z-direction. The computational domain spans $0 \leq r \leq 10$, $0 \leq \theta \leq 2\pi$, and $0 \leq z \leq 10$. A uniform resolution of 32 numeric cells over the initial jet radius is adopted. An out-

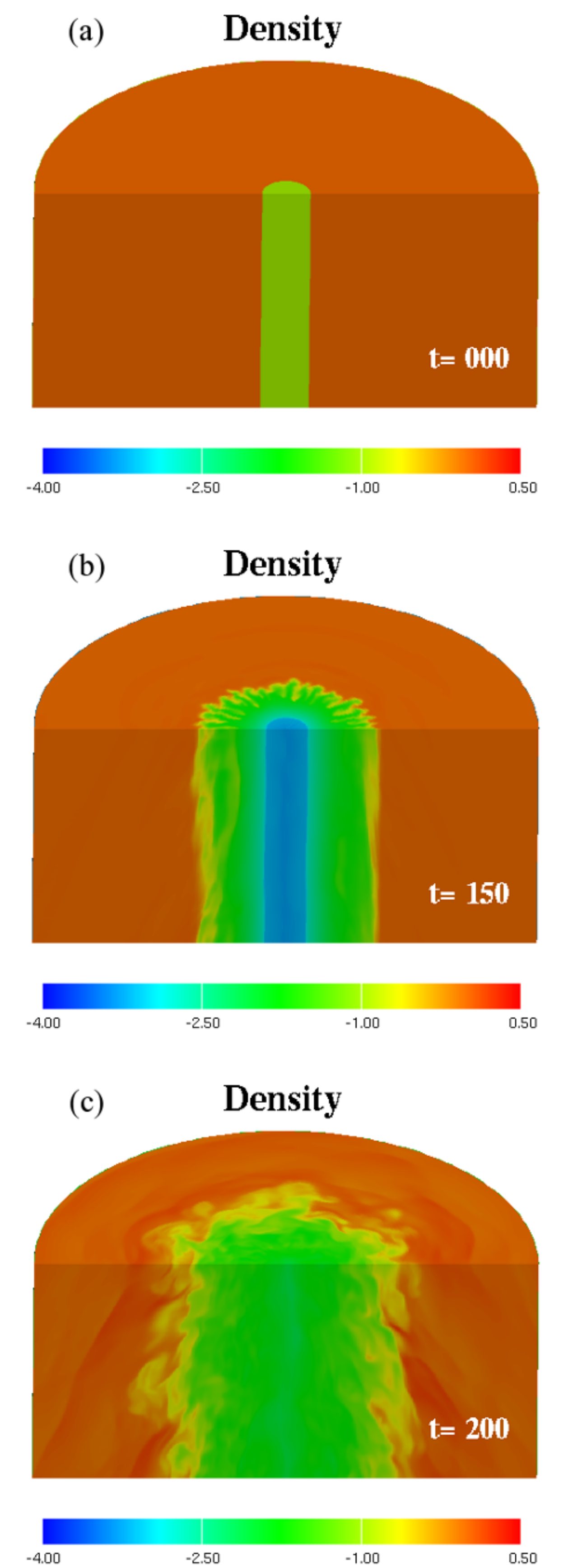

Figure 3. Three-dimensional density map of the jet-external medium system in the half simulation box modeling the radially oscillating motion of the jet when $t = 0$, 150, and 200.

flow (zero gradient) boundary condition is imposed on the outer boundaries of the grid (at $r = 10$). The calculation box is periodic along the axial (z) direction.

Figure 3 shows the temporal evolution of the 3D density map of the jet-external medium system in the half simulation box when $t = 0$, 150, and 200. In Figure 3(b), the inward-propagating reconfinement shock is formed behind the corrugated contact discontinuity that separates the jet and the external medium. A finger-like structure is a typical outcome of the Rayleigh-Taylor instability that is induced by inward pressure gradient force.

The convergence of the inward-propagating reconfinement shock produces an outward-spreading shock at the center of the jet. At the timing when the outward going shock collides with the contact discontinuity, the Richtmeier-Meshkov instability is secondarily excited between Rayleigh-Taylor instability fingers.

During the radial oscillating motion of the jet, the two types of finger structures are amplified and repeatedly excited at the contact discontinuity, and finally deform the transverse structure of the jet (see Figure 3(c)). The transverse structure of the jet is dramatically deformed by a synergetic growth of the Rayleigh-Taylor and Richtmeier-Meshkov instabilities once the jet-external medium interface is corrugated in the case with the pressure-mismatched jet.

Figure 4 shows the temporal evolution of the volume–averaged azimuthal velocity $|v_\theta|_{\rm ave}$ defined by

$$|v_\theta|_{\rm ave} = \frac{\int_{|v_z|>0} |v_\theta| \; r dr d\theta dz}{\int_{|v_z|>0} \; r dr d\theta dz} \ . \tag{4}$$

In this figure, the synergetic growth of the Rayleigh-Taylor and Richtmeier-Meshkov instabilities can be confirmed. The volume-averaged azimuthal velocity $|v_\theta|_{\rm ave}$ increases exponentially until $t \sim 80$ after $t \sim 25$. This is due to the Rayleigh-Taylor instability that grows at the jet-external medium interface. At around the time $t = 90$ when the outgoing shock passes through the contact discontinuity, the evolution property of the $|v_\theta|_{\rm ave}$ is dramatically changed, linearly increasing in time. This is evidence of the excitation of the Richtmeier-Meshkov instability because it is well-known that the perturbation amplitude grows linearly with time when the Richtmeier-Meshkov instability develops [27].

In addition, the condition for the transverse structure of the jet being maintained is studied by varying the initial effective inertia ratio between the jet and external medium, which is defined by

$$\eta_0 = \frac{\gamma_{\rm jet,0}{}^2 \rho_{\rm jet,0} h_{\rm jet,0}}{\rho_{\rm ext,0} h_{\rm ext,0}} \ , \tag{5}$$

through 2D numerical simulations in the r-θ plane modeling the nonlinear evolution of the jet cross section. Derivatives of the physical variables in the z-direction are dropped. See Matsumoto [24] for more detail of the settings of the 2D calculations.

We found that the stability criterion of the jet can be simply written as $\eta_0 \lesssim 1$. The jet can maintain its transverse structure as long as the effective inertia of the jet is

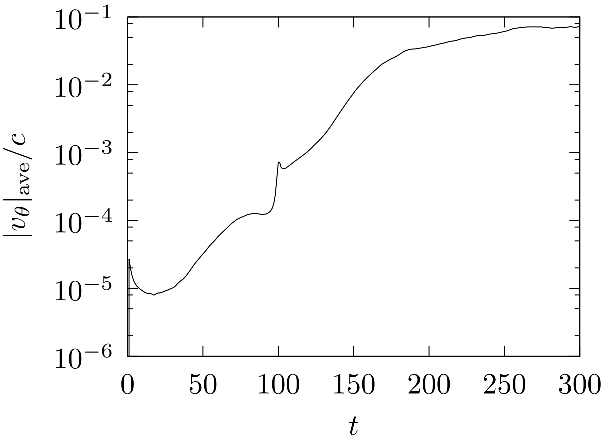

Figure 4. Time evolution of the volume-averaged azimuthal velocity $|v_\theta|_{\rm ave}$ defined by Equation (4).

smaller than that of the surround medium when excluding the destabilization effects by the Kelvin-Helmholtz mode along the jet direction.

The condition for the growth of the radial oscillation-induced Rayleigh-Taylor instability is the same as that for the centrifugally driven Rayleigh-Taylor instability found in Ref. [22]. This simply indicates that a contact discontinuity separating two fluids with $\eta_0 > 1$ becomes unstable to the Rayleigh-Taylor instability regardless of the origin of the driving force.

4 Summary

We investigate the nonlinear stability of the relativistically hot jet for the Rayleigh-Taylor and Richtmyer-Meshkov instabilities using 3D relativistic hydrodynamic simulations. The interface between the jet and surrounding medium is unstable to the Rayleigh-Taylor and Richtmyer-Meshkov instabilities when the relativistically hot jet propagates through the uniform ambient medium. These instabilities are induced by the radial inertia force that arises from a pressure mismatch between the jet and surrounding medium and is the restoring force of the radial jet oscillation. The cyclic in situ energy conversion between thermal energy and bulk kinetic energy of the jet is responsible for the radially oscillating motion of the jet.

The synergetic growth of the radial oscillation-induced Rayleigh-Taylor and Richtmyer-Meshkov instabilities triggers the deformation of the jet interface and the material mixing. The mixing between light faster jet and slow heavier external matters due to these instabilities leads to the deceleration of the jet.

From complementary two-dimensional simulations of transverse structure of the jet, we confirms that the stability criterion for the transverse structure of the jet to the z-axis is $\eta < 1$, where η is the effective inertia ratio of the jet to the external medium, when the relativistic jet interacts with the surrounding medium.

5 Acknowledgments

We thank Kazunari Shibata, Hiroyuki R. Takahashi, and Akira Mizuta for their useful discussions. Numerical computations were carried out on Cray XC30 at the Center for Computational Astrophysics, National Astronomical Observatory of Japan and on SR16000 at YITP at Kyoto University.

References

[1] Begelman, M. C., Blandford, R. D., & Rees, M. J., RvMP, **56**, 255 (1984)

[2] Ferrari, A., ARA&A, **36**, 539 (1998)

[3] Mirabel, I. F., & Rodríguez, L. F., ARA&A, **37**, 409 (1999)

[4] Piran, T., RvMP, **76**, 1143 (2004)

[5] Mészáros, P., RPPh, **69**, 2259 (2006)

[6] Marti, J. M. A., Mueller, E., Font, J. A., Ibanez, J. M. A., & Marquina, A., ApJ,**479**, 151 (1997)

[7] Gomez, J. L., Marti, J. M. A., Marscher, A. P., Ibanez, J. M. A., & Alberdi, A., ApJL, **482**, L33 (1997)

[8] Komissarov, S. S., & Falle, S. A. E. G., MNRAS, **297**, 1087 (1998)

[9] Mizuta, A., & Aloy, M. A., ApJ, **699**, 1261 (2009)

[10] Bromberg, O., Nakar, E., Piran, T., & Sari, R., ApJ, **740**, 100 (2011)

[11] Blandford, R. D., & Znajek, R. L., MNRAS, **179**, 433 (1977)

[12] Blandford, R. D., & Payne, D. G., MNRAS, **199**, 883 (1982)

[13] Uchida, Y., & Shibata, K., PASJ, **37**, 515 (1985)

[14] Nagataki, S., PASJ, **63**, 1243 (2011)

[15] Norman, M. L., Winkler, K.-H. A., Smarr, L., & Smith, M. D., A&A, **113**, 285 (1982)

[16] Sanders, R. H., ApJ, **266**, 73 (1983)

[17] Hardee, P. E., & Norman, M. L., ApJ, **334**, 70 (1988)

[18] Mizuno, Y., Hardee, P., & Nishikawa, K.-I., ApJ, **662**, 835 (2007)

[19] Perucho, M., Martí, J. M., Cela, J. M., et al., A&A, **519**, A41 (2010)

[20] Mizuno, Y., Lyubarsky, Y., Nishikawa, K.-I., & Hardee, P. E., ApJ, **700**, 684 (2009)

[21] Meliani, Z., & Keppens, R., A&A, **475**, 785 (2007)

[22] Meliani, Z., & Keppens, R., ApJ, **705**, 1594 (2009)

[23] Matsumoto, J., & Masada, Y., ApJL **772**, L1 (2013)

[24] Matsumoto, J., Masada, Y., & Shibata, K., ApJ, **751**, 140 (2012)

[25] Mignone, A., & Bodo, G., MNRAS, **364**, 126 (2005)

[26] Mignone, A., & McKinney, J. C., MNRAS, **378**, 1118 (2007)

[27] Nishihara, K.,Wouchuk, J. G., Matsuoka, C., Ishizaki, R., & Zhakhovsky, V. V., RSPTA, **368**, 1769 (2010)